https://doi 10.21608/bfszu.2019.15355.1002 BFSZU 1 (2019) 31-47

ASRT

Bulletin of Faculty of Science - Zagazig University

https://bfszu.journals.ekb.eg

FS-ZU

Using of Shallow Seismic Method for Evaluating the Foundation Beds of New Cairo Extension (Andalus Area), Egypt

Zaid, S. M.[1], Yousef, M. A. S.[2], Saad, A. M.[3], and Metwally, A. R.[1]

[1]Geology Department, Faculty of Science, Zagazig University, Zagazig, Egypt.

[2]Nuclear Materials Authority, Exploration Division, Po. Box 530, Maadi, Cairo, Egypt.

[3]Geology Department, Faculty of Science, Al-Azhar University, Cairo, Egypt.

ARTICLE HISTORY

Received: July/2019

Revised: September/2029

Accepted: November/2019

KEY WORDS

Shallow Seismic Refraction Method

wave velocity

geotechnical parameters

ABSTRACT:

Shallow Seismic Refraction Method (SSR) in engineering investigation is of growing interest after the October 1992 earthquake in Egypt. In the present study, eight shallow seismic refraction (SSR) profiles were acquired along Al-Andalus area, which is located at the southeastern part of the New Cairo extension, Egypt, in order to identify the shallow subsurface geological features of the near-surface section. Both the Primary (VP)-wave and Secondary (VS)-wave velocities, which were picked and computed during the processing and interpretation of the acquired data. The seismic compressional wave velocity (Vp) distribution indicates that, there are three geoseismic layers ranging between (420 and 680 m/s), (1040 and 1680 m/s) and (2170 and 3100 m/s), for the first, second and third layers, respectively. The first shear wave velocity (VS) is ranging between (240 and 390 m/s), the second VS layer ranging between (570 and 980 m/s) and the third VS layer is ranging between (1240 and 1800 m /s). The thickness of the first layer varies from 1.8 to 2.6 m and the second layer ranges between 7.6 and 10.5 m. The geoseismic cross sections are interpreted geologically, as the first low velocity layer which indicates weathered sediments of fine sands change to sandy gravels sometimes. However, the second geoseismic layer is represented by consolidated sands with clay intercalations, and the third layer reflects sandstones. The geotechnical parameters (elastic moduli, material competences and bearing capacities) are estimated. The distribution of these parameters relies that, the area can carry heavy loads at the central, east central and north central parts of the study area

***Corresponding Author:**

INTRODUCTION

New Cairo City lies in the southeastern part of the old Cairo, in the northern part of the Eastern Desert. The study area lies to the south east of great Cairo and covers an area of about 1.2×10^6 m^2. It is named "Al Andalus area" and is bounded by latitudes 29° 57` 28`` and 29° 58` 7``N, and longitudes 31° 31` 43`` and 31° 32` 35`` E (Fig.1).

The shallow seismic refraction technique is used for the purposes of engineering nowadays has increasing applications in the civil projects. The elastic properties, geotechnical parameters and bearing capacities of the subsurface layers can be determined from computing the Vp and Vs of the propagated seismic waves generated through subsurface layers (Grant and West, 1965). The soil mechanical properties depend on the elastic properties of the rock materials, which may be evaluated from the conventional techniques or from the geophysical measurements (e.g, Sjorgren et.al, 1979; Dutta 1984; Abd El Rahman et.al 1991 & 1992; Othman, 2005 and Arefa, et al., 2016). There are revealed that, shallow seismic refraction has evolved into a cost-effective tool for rapidly determining the geotechnical parameters in the engineering and construction projects.

The aim of the present study is to evaluate the foundation rock properties in the investigated area, by using seismic refraction measurements and their interpretation to estimate the seismic velocities for the layers and their thicknesses in each seismic profile, and the geotechnical parameters (Poisson's ratio, kinetic rigidity, modulus, Young's modulus, bulk modulus, material index, concentration index, stress ratio, ultimate and allowable bearing capacity) can be evaluated.

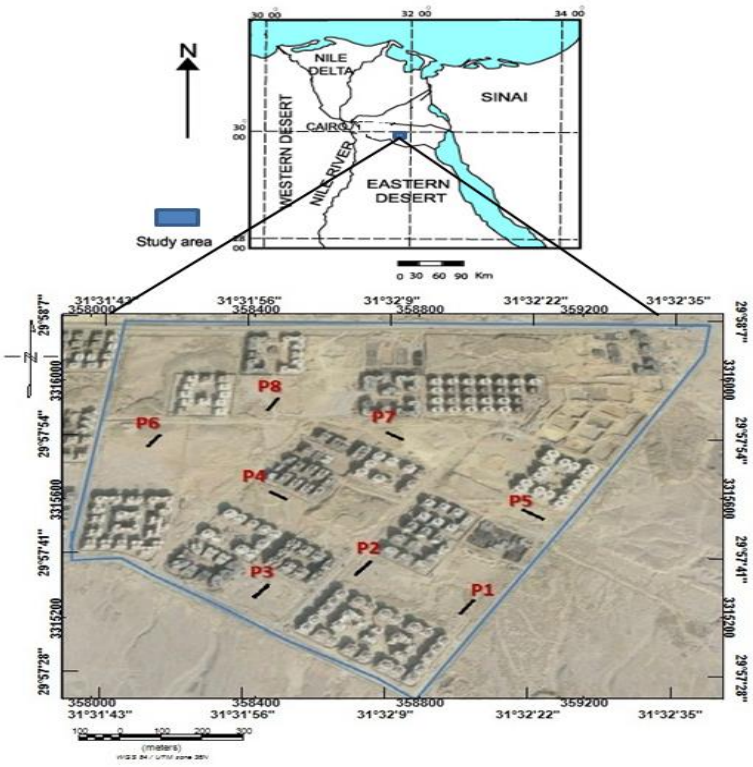

Fig.1: The location map of SSR profiles of the study area.

2. GEOLOGIC SETTING

The regional surface geology comprises different lithologic units belonging to Quaternary to Miocene. Figure (2) shows the geologic map of the New Cairo area (after Conoco, 1987). The new Cairo city shows different topographic units including: plateaux, wadis, lowlands and isolated hills. The study area belongs to the Upper Eocene rocks and the Oligocene rocks. The Upper Eocene rocks are represented by Maadi Formation (Said, 1960).

The Oligocene deposits are represented mainly by Gebel Ahmar Formation (Shukri, 1954). The Oligocene sediments are mainly composed of loose or weakly consolidated sands and gravels with large trunks of silicified wood. The sediments exhibit cross stratification, which are highly illustrated by the change of colors, reddish brown, brownish yellow and black. The Oligocene Gebel Ahmer Formation is widespread, covering a large stretch east and northeast of Gebel Mokattam e.g., Gebel El-Ahmer (type locality), Gebel Yahmoum El-Asmar, Gebel Nasuri, El Anqabia, Gebel Ikhshein and Bir Gindaly area. The Oligocene sediments were highly controlled by the structural and topographic lows, where a substantial thickness of these sediments was deposited, occupying several grabens and gently sloping areas between many synthetic faults (Shukri 1953; Shukri and Akmal 1953; and Al Ahwani 1982).

The Eocene (Maadi Formation) indicates the change of the depositional regime during the Bartonian and the Priabonian, and composed of sands and sandstones. Maadi is correlated with the Mokattam Stage (Zittel, 1883). The Maadi Formation is composed mainly of varicolored clastic sediments, shale, sandstones and fossiliferous yellowish white marly limestone and other oyster banks (Nassif et al., 2018). The Maadi Formation overlies the Mokattam Formation and underlies the Oligocene sediments (Said, 1962). The Gebel Ahmer Formation unconformably overlies the Upper Eocene Maadi Formation and uncomfortably underlies the Miocene sediments or basalt sheets.

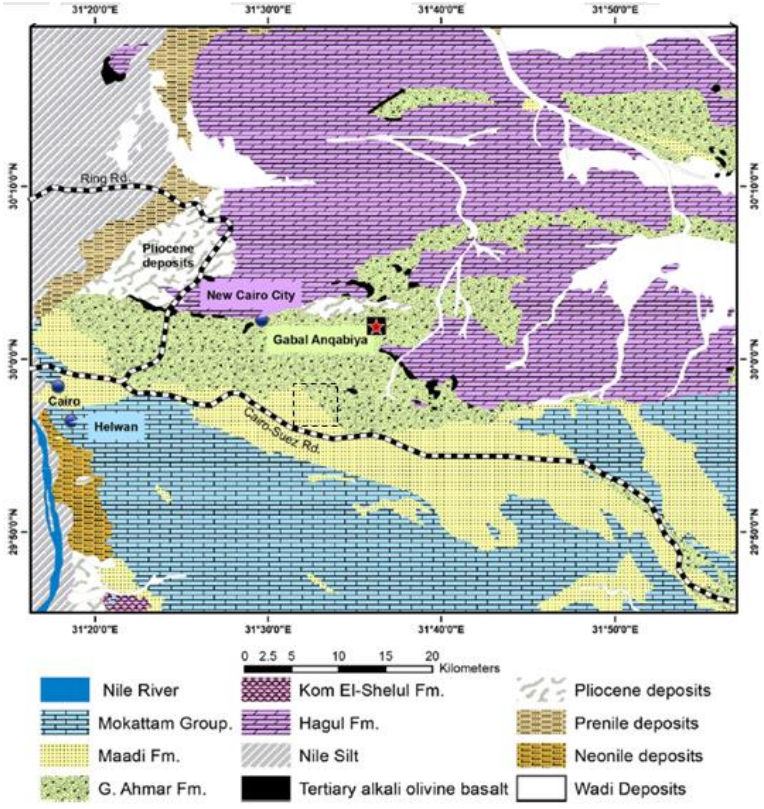

Fig.2: Geologic map of the New Cairo City (modified after Conoco, 1987)

3. Material and Methods

3.1 Shallow Seismic Refraction data acquisition

Seismic refraction method uses the seismic energy, which returns back to the surface, after traveling through the shallow ground along refracted ray-paths. The first arrivals of the seismic waves to geophone offsets from a seismic source always represent either direct rays or refracted rays (Sharma, 1997). In general, the compressional wave and shear wave velocities increase with the confining pressure and increasing depths. SSR was carried out,

using the Strata View^{TM} data logger and though with 48 highly sensitive vertical and horizontal geophones, and a sledge Hammer energy source of 15 kg. Two off-end spreads (forward and reverse) were designed for this survey, according to the geologic information and the aim of study, in addition to two offset spreads and one split spread; with one meter as geophone spacing. Eight seismic spread sites (SP) are distributed regularly through the study area with varying directions (Fig.1).

3.2. Shallow seismic refraction analysis and interpretation

The results obtained from the shot records and their interpretation show that, the study area reflected three geoseismic layers. The velocity values of the first geoseismic layer indicate weathered sediments (sands and sandy gravel) at the top, which has thickness is varies between 1.5 m and 2.6 m. The second geoseismic layer velocities correspond to (sand and clay intercalation) and having thickness varies between 8.5 m and 10.5 m. The third geoseismic layer is characterized by high seismic velocity, which corresponds to sandstone, where the results of the interpretation for all the spreads reveal three layers model almost like each other. Figures 3A and 3B show examples to the time-distance curves and geoseismic cross-sections of the compressional and shear waves, respectively, along profiles No.3.

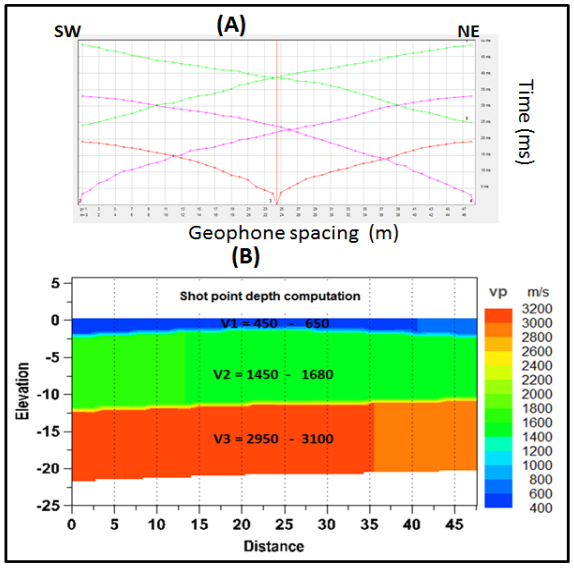

Fig. 3A: Travel time-distance curve of compression waves (A) and its geoseismic cross section (B) at P3.

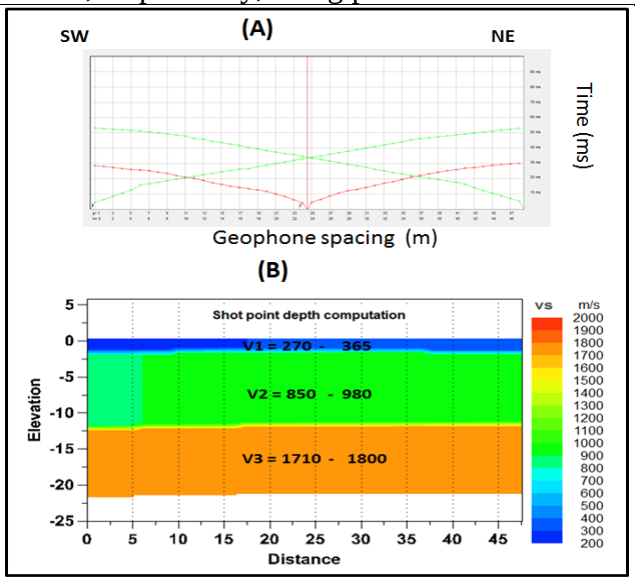

Fig. 3B: Travel time-distance curve of shear waves (A) and its geoseismic cross section (B) at P3.

3.3. Shallow seismic refraction presentation

3.3.1Compressional seismic velocities (Vp)

The seismic primary wave velocity distribution is represented within three geoseismic layers (Figs. 4a, 4b and 4c), respectively. Where, the P-wave in the first geoseismic layer (Fig. 4a) has maximum values located at the central (P4) and east parts (P6) of the study area. On the other hand, the minimum values are located at the northern (P7) and southern parts (P1 and P2) of the study area. The P-wave velocities of the second geoseismic layer (Fig. 4b) have maximum values at the central (P3) and eastern parts (P6) of the study area. Meanwhile, the minimum values at the southwestern part (P2) of the study area. The third geoseismic layer has high Vp-wave at the central part (P3, P4 and P7) of the study area (Fig. 4c), while the Vp_3 decreases toward the southern (P1 and P2) and western sides (P5).

3.3.2. Layer thicknesses

The maximum thickness of the first layer is recorded at the northern part of the study area (P7), while the thickness of this layer decreases toward the southeastern (P1) and northwestern parts (P5). The maximum thickness of the second geoseismic layer lies at the central part of the study area (P3 and P4), while the thickness decreases toward the

southeastern part (P1). Table (1) summarizes the Vp velocities range for the three subsurface layers and their thicknesses.

3.3.3. Shear seismic velocities (Vs)

The S-wave in the first geoseismic layer (Fig. 5a) has maximum values located at the central (P4) and eastern parts (P6) of the study area. On the other hand, the minimum values are located at the northern (P7) and southern parts (P1 and P2) of the study area. The S-wave velocities of the second geoseismic layer (Fig. 5b) have maximum values at the central (P3 and P4) and east parts (P6) of the study area. Meanwhile, the minimum values are located at the southwestern part (P2) of the study area. The third geoseismic layer (5c) has high Vs-waves at the central part (P3, P4 and P8) of the study area, while the Vs of the third geoseismic layer decreases toward the southern (P1 and P2) and western sides (P5). Figs (5a, 5b and 5c) show the S-wave distribution maps for the first, second and third layers, respectively.

3.3.4. Layer densities

The maximum densities of the first geoseismic layer are recorded at the central and eastern parts of the study area (P6), while the densities of this layer decreasing toward the southern (P1, P2) and northern parts (P7). The maximum densities of the second geoseismic layer are noticed at the central and northern parts of the study area (P3, P6 and P7), while the densities are decreasing toward the southern part (P1 and P2). Table (2) summarizes the shear wave velocities and rock densities of the subsurface layers of the study area.

Table1: The Primary wave velocities for the layers and their thicknesses and depths

profile No.	Primary wave velocity (m/s)						Thickness (m)	
	VP_1		VP_2		VP_3		T_1	T_2
1	480	580	1220	1420	2320	2620	1.5	8.5
2	430	500	1040	1120	2170	2550	2.5	10.1
3	450	650	1450	1680	2950	3100	2.3	10.2
4	540	675	1260	1440	2650	3010	1.7	10.5
5	500	600	1150	1310	2220	2580	1.5	9.7
6	580	680	1450	1620	2530	2790	1.8	9.5
7	420	480	1070	1210	2685	2900	2.6	9.8
8	490	550	1120	1380	2785	2940	2.1	10

Table2: The Shear wave velocities and their rock densities for the three layers

profile No.	Shear wave velocity (m/s)						Rock density (g/cc)		
	VS_1		VS_2		VS_3		$\dot{\rho}_1$	$\dot{\rho}_2$	$\dot{\rho}_3$
1	280	360	660	750	1330	1450	1.47	1.87	2.19
2	240	280	570	640	1240	1350	1.47	1.78	2.16
3	270	365	850	980	1710	1800	1.5	1.96	2.3
4	320	390	855	965	1520	1670	1.54	1.88	2.26
5	280	380	660	750	1280	1500	1.5	1.84	2.17
6	340	390	810	930	1500	1620	1.55	1.94	2.23
7	245	275	620	670	1490	1680	1.44	1.8	2.25
8	300	350	740	790	1640	1680	1.48	1.84	2.27

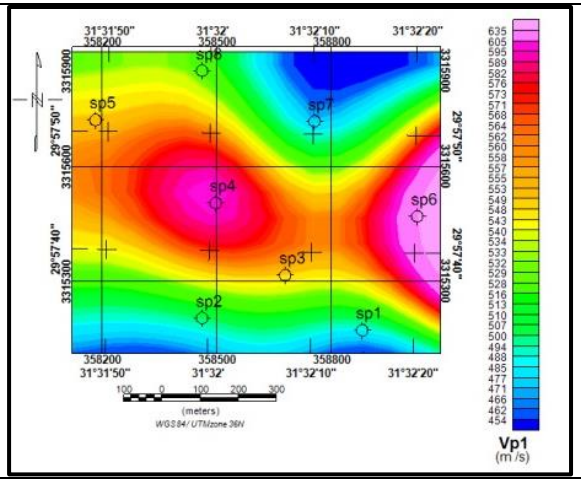

Fig.4a: P-wave colored image of the first layer in the spot area

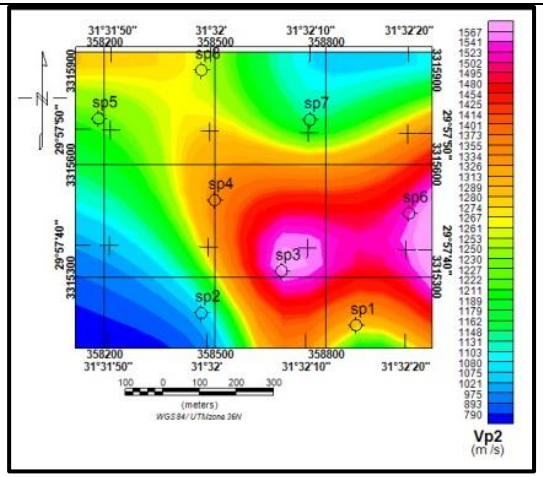

Fig.4b: P-wave colored image of the second layer in the spot area

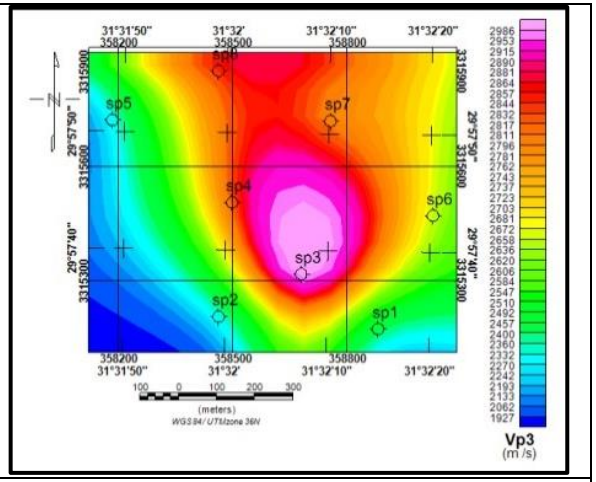

Fig.4c: P-wave colored image of the third layer in the spot area

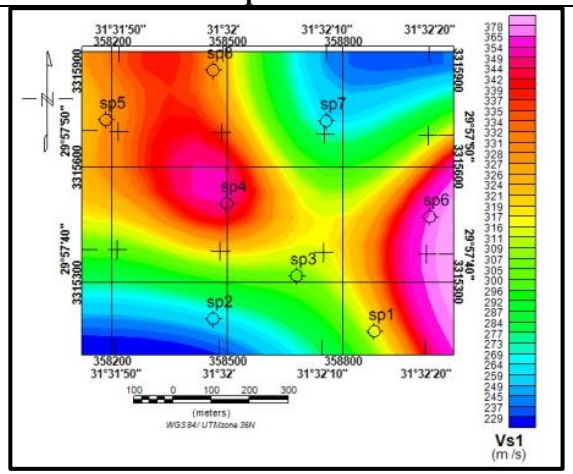

Fig.5a: S-wave colored image of the first layer in the spot area

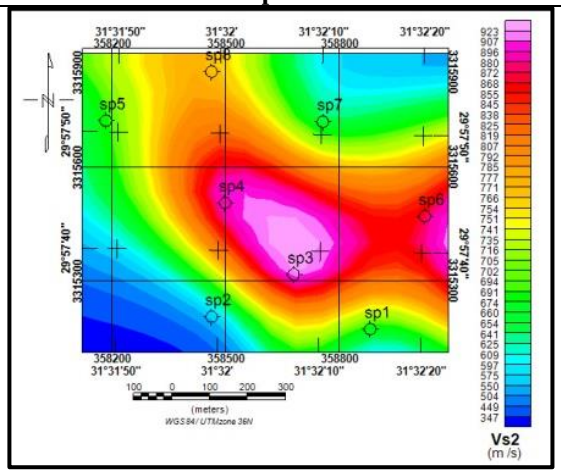

Fig.5b: S-wave colored image of the second layer in the spot area

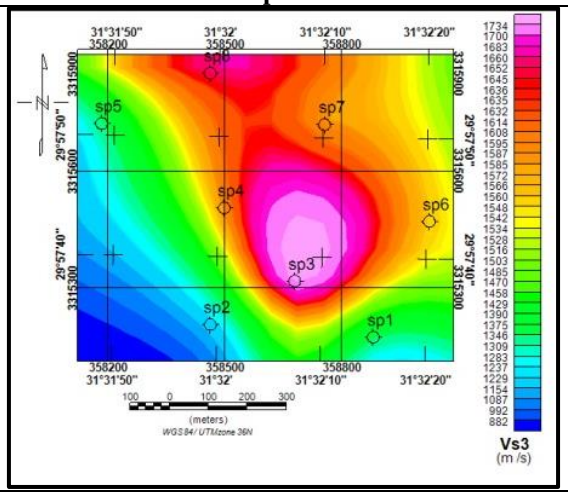

Fig.5c: S-wave colored image of the third layer in the spot area

4. GEOTECHNICAL CHARACTERISITICS OF THE FOUNDATION MATERIAL

Knowledge of the seismic velocities is important in engineering considerations, because the P-wave and S-wave velocities are controlled by the fundamental parameters of the elastic strength and density. The physicomechanical properties of a rock material, such as the dynamic elastic modulus, competence scales and bearing capacities can be utilized to provide direct information about the rock materials quality (Kelly and Mares, 1993). Koefoed (1955) studied the effect of Poisson's ratio on the reflection coefficients of the seismic waves. Brace (1965) measured the compressibility of some rocks. Kaarsberg (1966) determined the elastic constants of an isotropic solid, applying the plate velocity measurements. Schreiber *et al* (1973) published a book about the elastic constants, describing the different measuring techniques.

4.1 ELASTIC MODULI:

4.1.1. Poisson's Ratio (σ):

It is simply related to the velocity squared ratio (Vs^2/Vp^2) by the following equation, according to **Telford et al (1976)**.

$$\sigma = \frac{(1-2\left(\frac{Vs^2}{Vp^2}\right))}{2(1-\left(\frac{Vs^2}{Vp^2}\right))} \quad \text{…….. (1)}$$

The Poisson's ratio in the first geoseismic layer is shown in Fig. (6a). The maximum value (0.32) is located at the southwestern part of the study area, while the minimum values are noticed at the southeast of the area. The second geoseismic layer (Fig. 6b) shows maximum values (more than 0.300) located at the southern part of the study area and minimum values (less than 0.20) located at the central and north-central parts of the study area. The Poisson's ratio of the third geoseismic layer (Fig. 6c) has maximum values (more than 0.32) located at the southwestern part of the study area, and has minimum values (0.24) noticed at the eastern and northwestern parts of the study area, which indicate moderately competent to competent materials.

4.1.2 Kinetic Rigidity Modulus (μ);

The shear or rigidity modulus (μ) is defined from the shear deformation. It is a measure of the stress/strain ratio in the case of a simple tangential stress, **(Sharma, 1997)**. The shear modulus is given by the following formula:

$$\mu = \rho Vs^2 \quad \text{…….. (2)}$$

Shear modulus distribution of the study area is shown in Figs. (7a, 7b and 7c) for the first, second and third geoseismic layers, respectively. The high value 2.07×10^9 dyne/cm^2 of the first layer is locate in the eastern and central part of the study area, while the lowest value 0.98×10^9 dyne/cm^2 is located at the northeastern and southwestern parts of the study area. The second geoseismic layer has the highest value 16.75×10^9 dyne/cm^2 at the central and eastern parts of the study area, while the lowest value 5.88×10^9 dyne/cm^2 is occurred at the southwestern part of the study area. The shear modulus in the third geoseismic layer has high value 70.81×10^9 located at the central and northcentral parts of the study area, meanwhile the low value 32.42 dyne/cm^2 located at the southwestern part of the study area.

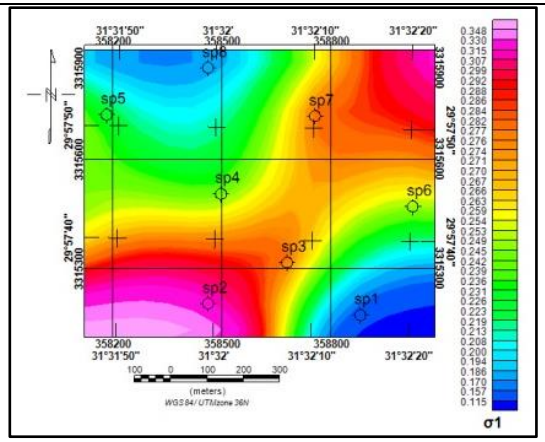

Fig.6a: Poisson′s Ratio (σ) colored image of the first layer in the spot area.

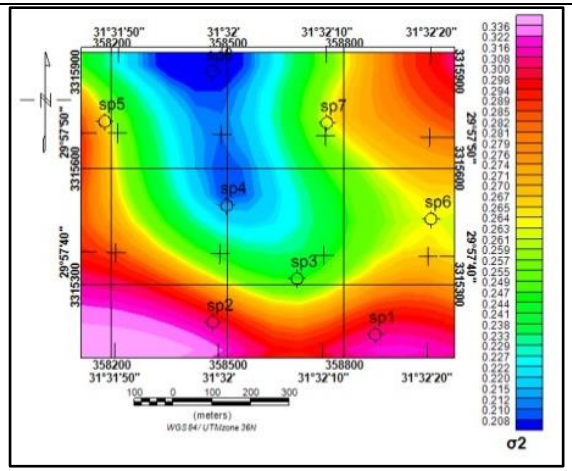

Fig.6b: Poisson′s Ratio (σ) colored image of the second layer in the spot area

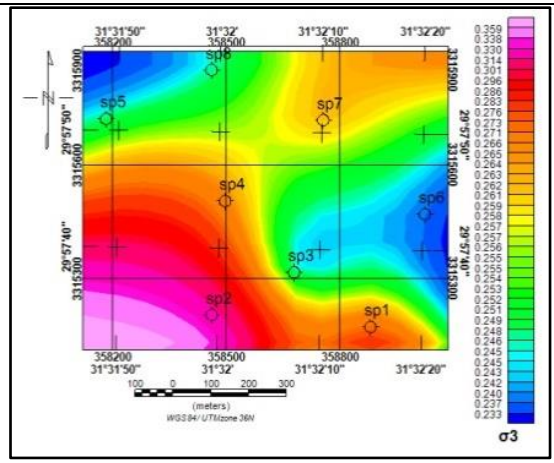

Fig.6c: Poisson′s Ratio (σ) colored image of the third layer in the spot area

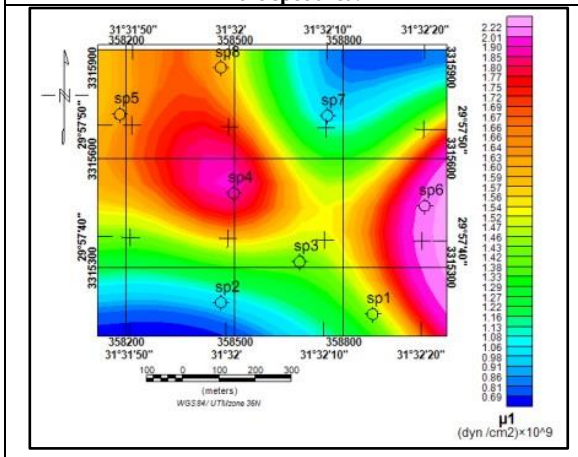

Fig.7a: shear modulus (μ) colored image of the first layer in the spot area.

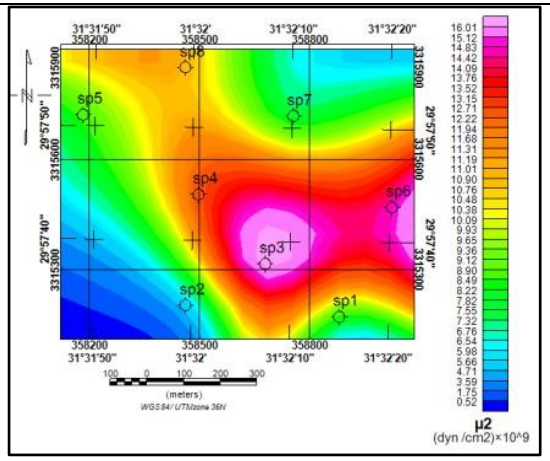

Fig.7b: shear modulus (μ) colored image of the second layer in the spot area.

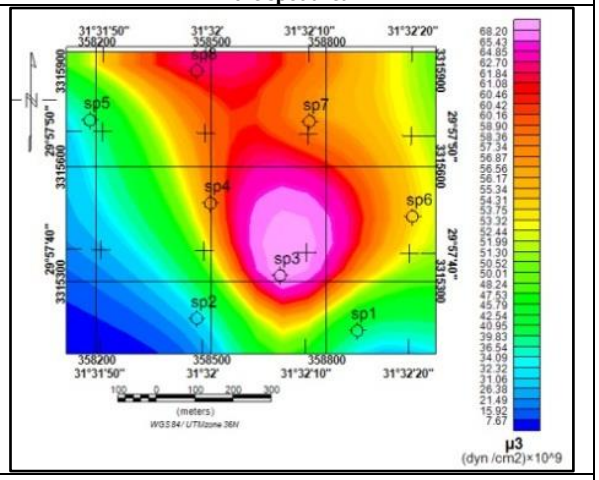

Fig.7c: shear modulus (μ) colored image of the third layer in the spot area.

4.1.3 Young's modulus (E)

It is a linear behavior over some parts of stress and the corresponding strain. Soil exhibits linear stress and strain characteristics and given by **Bowles (1984)**. The conventional terminology of the modulus of elasticity is the kinetic deformation coefficient and formulated as a function of the rigidity modulus and Poisson's ratio by **Imai et al. (1976)** as follows:

$$E = 2\mu(1+\sigma) = \rho V^2 \frac{2(1+\sigma)(1-2\sigma)}{(1-\sigma)} \quad \ldots\ldots\ldots\ldots\ldots\ldots (3)$$

The kinetic young's modulus distribution of the first geoseismic layer (Fig. 8a) shows high value of 5.16×10^9 dyne/cm^2 at the eastern and central parts of the study area, while the lowest value 2.50 dyne/cm^2 is shown at the southwestern part of the area. The young's modulus of the second geoseismic layer (Fig. 8b) exhibits high value of 37.11×10^9 dyne/cm^2 at the central and eastern parts of the study area, while the lowest value 15.30 dyne/cm^2 is at the southwestern part of the study area. The third geoseismic layer shows high kinetic young's modulus value of 176.50×10^9 at the central part of the study area, while the low kinetic young's modulus value 85.31 dyne/cm^2 appears at the southwest of the study area (Fig. 8c).

4.1.4 Kinetic Bulk Modulus (K)

The bulk modulus (K) is defined as the ratio between the stress and the strain in case of a simple hydrostatic pressure, which produces a change in the volume. In other words, it is a measure of the capacity of a substance to be compressed (Robinson, 1988) and given by the following formula:

$$K = \frac{E}{3(1-2\sigma)} \quad \ldots\ldots\ldots\ldots (4)$$

Figures 9a, 9b and 9c show the bulk modulus of the first, second and third geoseismic layers at the study area the first layer has Kinetic Bulk Modulus (9a) ranges between 1.66 × 10^9 dyne /cm^2 and 3.40 x 10^9 dyne /cm^2, while the Kinetic Bulk Modulus of the second layer (9b) ranges between 12.88 x 10^9 dyne /cm^2 and 27.13 × 10^9 dyne/cm^2. The third geoseismic layer (9c) has Kinetic Bulk Modulus ranges between 69.01 × 10^9 dyne /cm^2 and 115.85 x 10^9 dyne /cm^2. These maps show the highest elastic modulus, which located at the central, eastern and northeastern parts of the study area.

4.2. Rock Material Competence Scale:

4.2.1. Material Index (Mi):

The material index is an expression introduced by ***Abd El-Rahman (1989)*** to define the material quality from the foundation point of view. It addresses the degree of material competence on the basis of their elastic moduli. This index has relations to the factors, which affect the elastic moduli, such as mineral composition, the degree of consolidation, fracturing and fluid saturation. ***Abd El-Rhaman (1989)*** derived a mathematical expression of the material index in terms of Lame's constant and Poisson's ratio as follows:

$$Mi = (\mu - 1)/(\lambda + \mu) = (1 - 4\sigma) \quad \ldots\ldots\ldots\ldots (5)$$

The material index of the first geoseismic layer is characterized by high values (0 - 3.88) at the northwestern and southeastern parts of the area (10a) which reflected competent materials, meanwhile the rest of the concerned area is characterized by low material index (-0.259 - 0), which reflected fairly to moderately competent materials. The second layer shows high material index of (0.023 – 0.196) at the central and eastern parts of the study area (Fig.10b), which reflected competent materials, while the low material index of (-0.209 - -0.022) is shown at the rest of the concerned area,

which reflected fairly to moderately competent materials. The high material index of the third layer (0.010 – 0.049) are noticed at the eastern and northwestern parts of the study area, which reflected competent materials, while the low material index of rocks (-0.262 - -0.049) are shown at the rest of the concerned area, which reflected fairly to moderately competent materials (Fig. 10c).

4.2.2. Concentration Index (Ci):

Bowless (1984) described the degree of material concentration or compaction by the parameter (C_i). Rock or soil compaction status is considered as a measure of the degree of competence for foundation and other civil engineering purposes. The concentration index can be expressed in terms of Poisson′s ratio **(*Bowless, 1984)*** as:

$$Ci = ((1+\sigma)/\sigma) \quad \text{..... (6)}$$

Or may be expressed by (Vs^2 / Vp^2***) (Abd El-Rahman, 1991)*** *as*:

$$Ci = \frac{[3-4\left(\frac{Vs^2}{Vp^2}\right)]}{[1-2\left(\frac{Vs^2}{Vp^2}\right)]} \text{..... (7)}$$

Figures 11a, 11b and 11c show the concentration index of the first, second and third geoseismic layers. The Ci of the first geoseismic layer varies from 4.18 to 7.53, where the highest values are shown in the northwestern and southeastern parts of the study area and the lowest values are noticed elsewhere. However, the Concentration Index of the second geoseismic layer has range from 4.33 to 5.99. The highest values are noticed at the central and extended to the north northwest part of the study area and the lowest values are located at the other parts of the study area. The concentration index in the third geoseismic layer varies from 4.17 to 5.20. The highest values of Ci are located at the eastern and the northwestern parts of the study area, which indicate fairly compacted to compacted material in the first layer and fairly compacted to moderately compact in the second and third layers.

4.2.3. Stress Ratio (Si):

The stress ratio (Si) can be represented as the relation between the vertical stress at a certain depth and the horizontal stress, due to the pore filling fluids and can be estimated, using the following formula **(Thomson, 1986)**.

$$Si = \delta / (1-\delta) \quad \text{..... (8)}$$

The propagation of seismic waves is proportional to the differential pressure between the sedimentary overburden and the pour filling fluids. This means that, the high fluid pressure formations will have low differential pressure and consequently abnormally low seismic wave velocities. The stress ratio can also be expressed in terms of the velocity squared ratio, as follows:

The stress ratio in the first geoseismic layer (Fig.12a) is ranged between 0.19 and 0.46, where the high values are located at the southwestern and northeastern parts, while the lowest values are located at the other parts of the study area, which indicate highly competent to fairly competent. The Si of the second geoseismic layer (Fig.12b) is ranged from 0.25 to 0.43. Its highest values are shown at the southwestern and southeastern parts of the study area, which reflected highly competent to moderately competent. The Si of the third geoseismic layer (Fig. 12c) is ranged from 0.312 to 0.46, where the highest values located at the southwest of the study area and reflected moderately competent to fairly competent status.

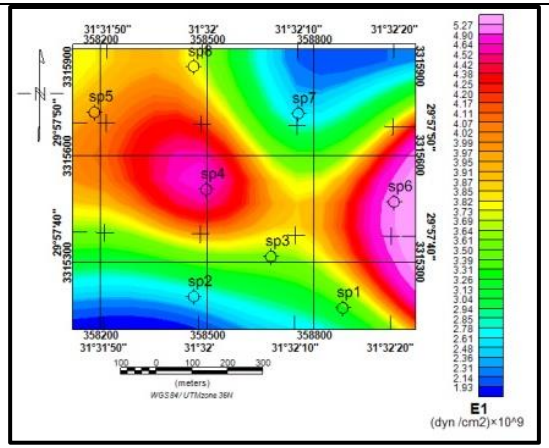

Fig.8a: Kinetic Young's Modulus (E) colored image of the first layer in the spot area.

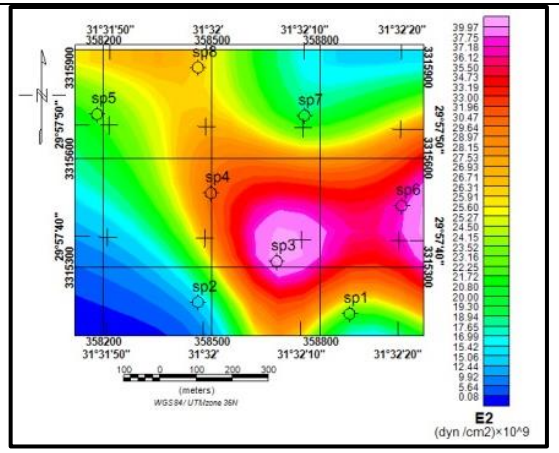

Fig.8b: Kinetic Young's Modulus (E) colored image of the second layer in the spot area.

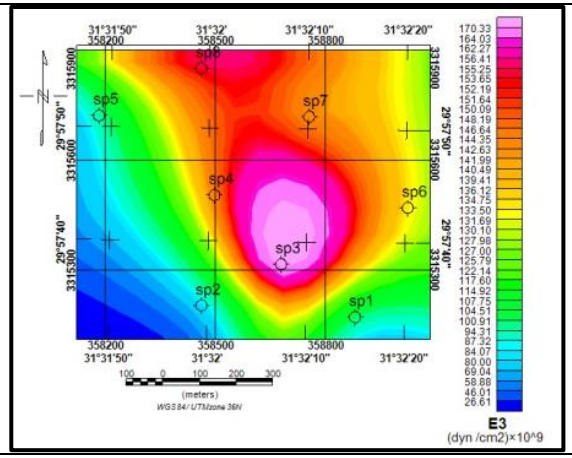

Fig.8c: Kinetic Young's Modulus (E) colored image of the third layer in the spot area.

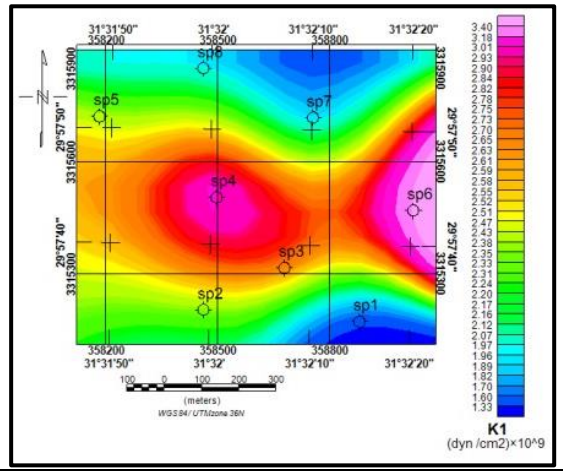

Fig.9a: Bulk Modulus (K) colored image of the first layer in the spot area.

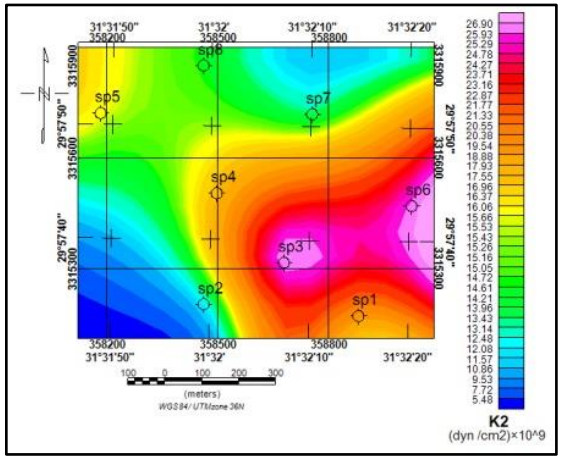

Fig.9b: Bulk Modulus (K) colored image of the second layer in the spot area.

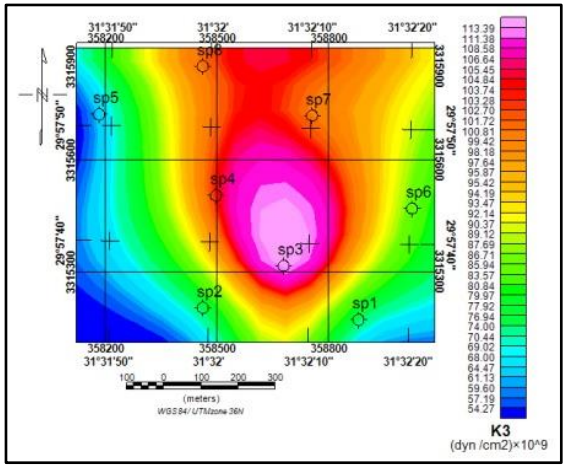

Fig.9c: Bulk Modulus (K) colored image of the third layer in the spot area.

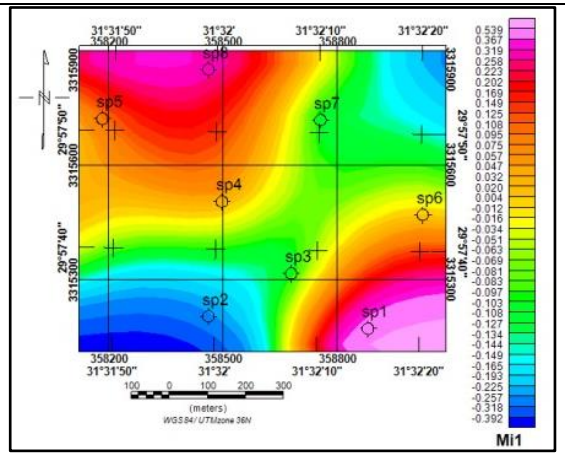

Fig.10a: Material Index (Mi) colored image of the first layer in the spot area.

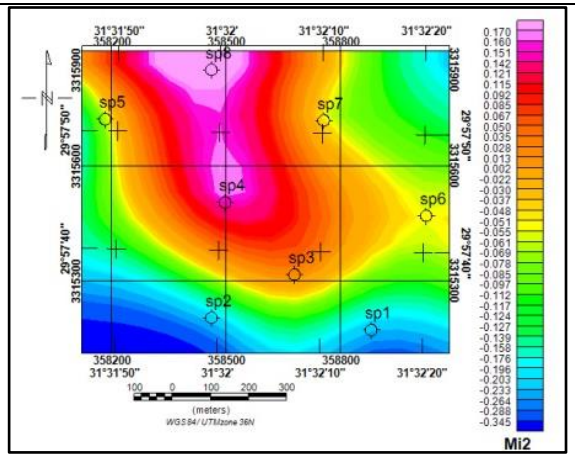

Fig.10b: Material Index (Mi) colored image of the second layer in the spot area.

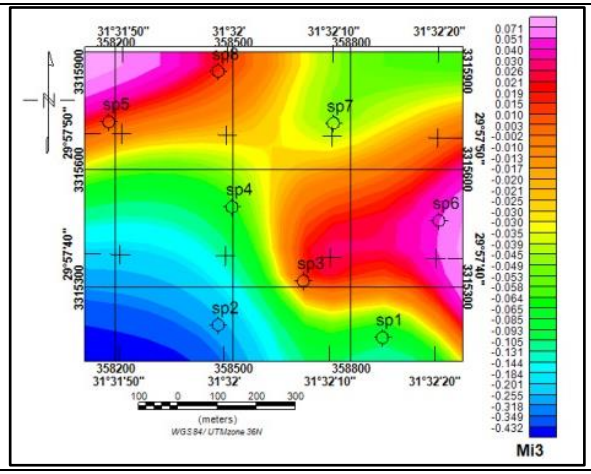

Fig.10c: Material Index (Mi) colored image of the third layer in the spot area.

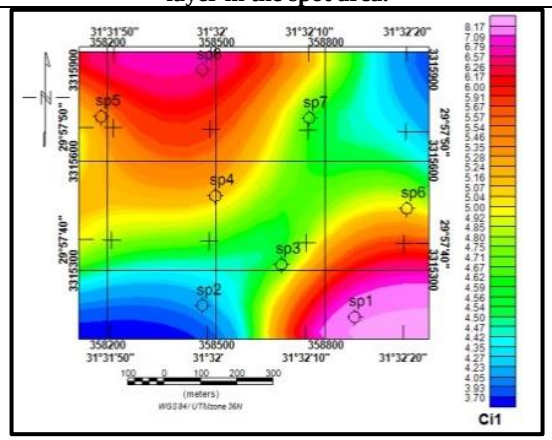

Fig.11a: Concentration Index (Ci) colored image of the first layer in the spot area.

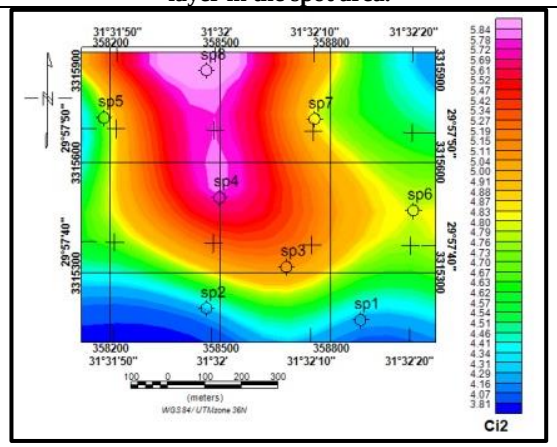

Fig.11b: Concentration Index (Ci) colored image of the second layer in the spot area

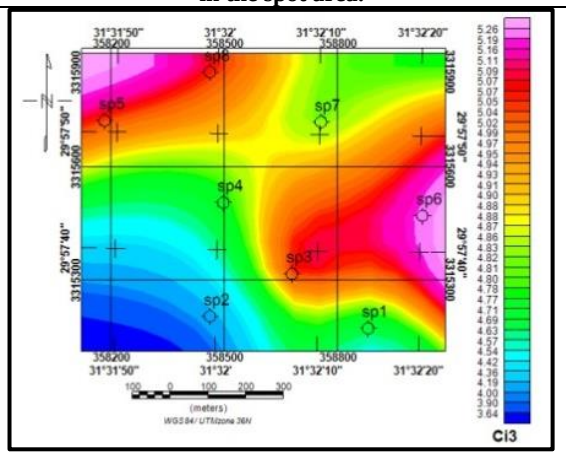

Fig.11c: Concentration Index (Ci) colored image of the third layer in the spot area

4.3. FOUNDATION MATERIALS BEARING CAPACITY

4.3.1 Ultimate-Bearing Capacity (Qult):

The ultimate bearing capacity is defined as the maximum load required for shear failure or sand liquefaction. Most of the currents used bearing capacity theories are based on the plasticity theory. The ultimate-bearing capacity of cohesionless materials can be evaluated, using the standard penetration test (SPT), according to ***Parry's Formula (1977)*** as:

$$Q_{ult} = 30\ N \qquad \ldots\ldots\ldots (10)$$

Where: N is the resistance to penetration by normalized cylindrical bars under standard load, ***Abd El-Rahman (1991)*** derived a relation between the ultimate-bearing capacity and shear wave velocity;

$$Q_{ult} = 10^{2.932} (\log V_s - 1.45) \qquad \ldots\ldots\ldots (11)$$

The distributions of the ultimate bearing capacity of the first, second and third geoseismic layers are shown in figures 13a, 13b and 13, respectively. The ultimate-bearing capacity in the first geoseismic layer is characterized by the minimum value (0.67kg/cm^2), which located at the southwestern part of the study area, and the maximum value (1.82 kg/cm^2)appears at the east part of the study area. The second geoseismic layer has high ultimate-bearing capacity of high values (more than 25.88 kg/cm^2) at the central and eastern parts of the study area, while the lowest value 6.92 kg/cm^2 is located at the southwest of the study area. The ultimate-bearing capacity of the third geoseismic layer has high value of 182.31kg/cm^2 at the central part of the study area, meanwhile the lowest value of 63.54kg/cm^2 is noticed at the southwest of the study area, in which the higher bearing capacity value at a site indicates a higher material quality at that site and vice versa.

4.3.2. Allowable Bearing Capacity (Q_a):

It is the maximum load considered to avoid shear failure or sand liquefaction. It can be reduced from the Q_{ult} by a suitable factor of safety F. This safety factor is equal to 2 for the cohesionless soil and F = 3 for the cohesive soil ***(Parry, 1977)***.

$$Q_a = Q_{ult} / F \qquad \ldots\ldots\ldots (12)$$

Figures 14a, 14b and 14c show the calculated values of the allowable-bearing capacity in Kg/cm^2 for the three subsurface layers. The allowable-bearing capacity in the first geoseismic layer is ranged from 0.34 kg/cm^2 to 0.91 kg/cm^2, while Q_a in the second geoseismic layer ranges between 3.46 and 13.94 kg/cm^2, and in the third layer the allowable-bearing capacity varies from 31.77 kg/cm^2 to 91.16 kg/cm^2, the higher allowable-bearing capacity values are noticed at the central, north central and east central parts of the study area, that indicate higher material quality to carry a heavy loads and vice versa.

Figure 15 shows the configuration of the competence loads, based on the integration of velocities, elastic moduli, material competences and bearing capacities distribution maps. The higher allowable-bearing capacity values are indicate to parts having high values of Vp, Vs, Mi, Ci, Qult, K, E and μ at a site indicate higher material carried heavy loads and vice versa.

5. Summery and Conclusions

From shot records (acquisition field), velocity computation and analysis (processing data) and their interpretation show that, the Andalus area reflected three geoseismic layers. The Vp values of the first layer (420 - 680 m/s) indicate weathered layer (sands with some gravel) at the top, which has thickness varies between 1.5 m

and 2.6 m, Vs range (240 - 390m/s), while the second geoseismic layer has Vp range (1040 - 1680 m/s) corresponds to (sand and clay intercalations), with thickness of this layer varies between 8.5 m and 10.5 m and having Vs range (570 – 980 m/s). The third geoseismic layer is characterized by Vp range (2170 - 3100 m/s) and having Vs range (1240 - 1800 m/s), that corresponds to (sandstone).

The elastic moduli of the geotechnical parameters (Poisson's ratio, kinetic rigidity modulus (μ), Young's modulus (E) and Bulk modulus (K) distribution maps show that, The highest values of the elastic moduli through the first geoseismic layer is located at the eastern, central and north central parts of the study area, while the lowest values are located at the southwestern part of the study area. the second geoseismic layer has high values of elastic moduli at the central and eastern parts of the study area, while the lowest values appear at southwest of the study area. The third geoseismic layer have high values inhibited noticed at the central and north central parts of the study area, while the lowest values are exhibited the southwestern part of the study area.

The competence scales of the geotechnical parameters across the concerned area (Mi, Ci and Si) are computed for the three subsurface layers. The distribution of the highest values appear at the northwestern and southeast parts for the first geoseismic layer, at the central and north central parts for the second geoseismic layer, and at the east central and northwestern parts for the third geoseismic layer, however, the rest of the considered parts are characterized by low values. The stress ratios of the three layers are characterized by moderately competent to competent materials.

The ultimate- and allowable- bearing capacities are computed revealing that, the area can be carried heavy loads at the central, east central and north central parts of the study area. The higher allowable-bearing capacity values are associated with parts having high values of Vp, Vs, Mi, Ci, Qult, K, E and μ at a site indicating higher material carried heavy loads and vice versa.

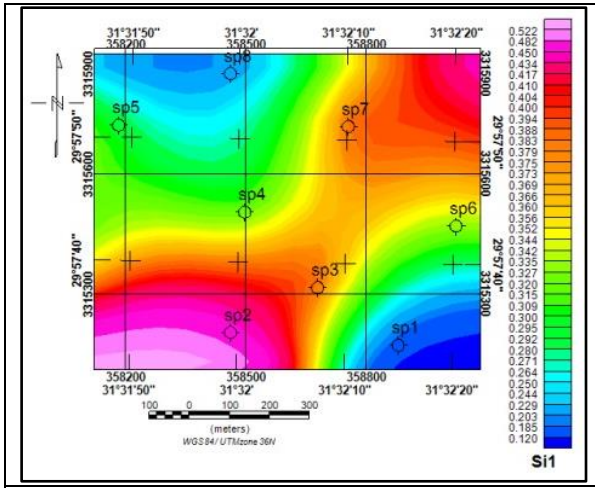

Fig.12a: Stress Ratio (Si) colored image of the first layer in the spot area

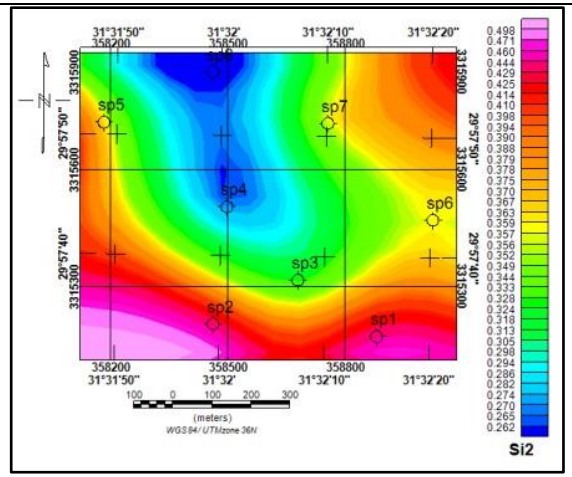

Fig.12b: Stress Ratio (Si) colored image of the second layer in the spot area

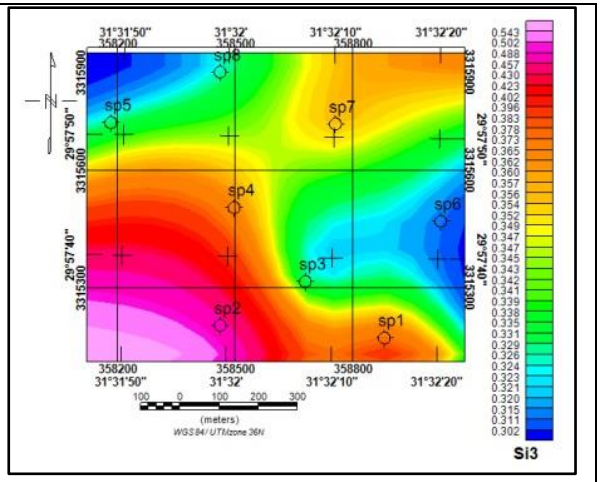

Fig.12c: Stress Ratio (Si) colored image of the third layer in the spot area

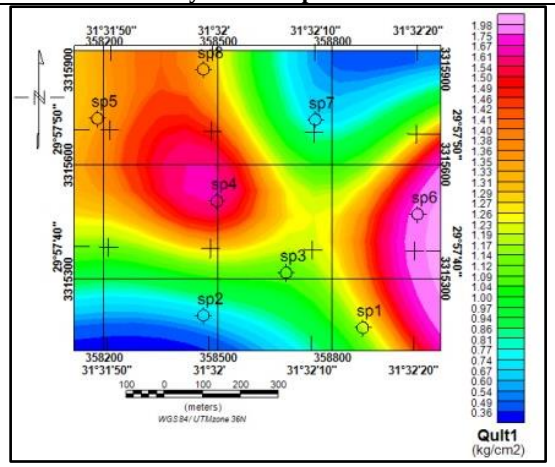

Fig.13a: Ultimate Bearing Capacity colored image of the first layer in the spot area.

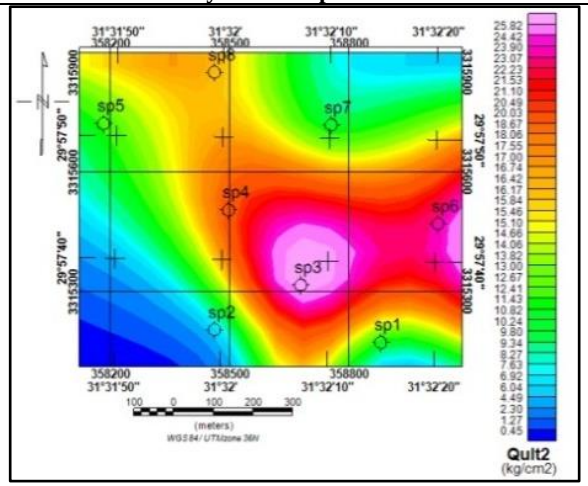

Fig.13b: Ultimate Bearing Capacity colored image of the second layer in the spot area.

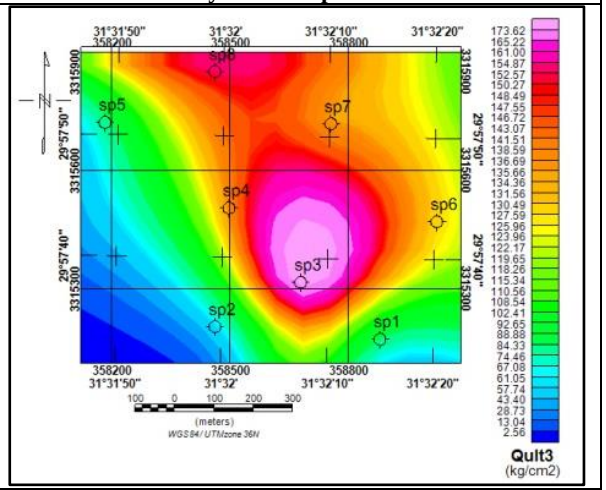

Fig.13c: Ultimate Bearing Capacity colored image of the third layer in the spot area.

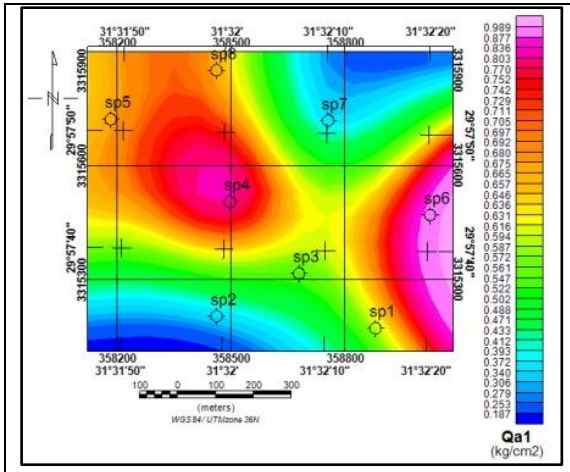

Fig.14a: Allowable Bearing Capacity colored image of the first layer in the spot area.

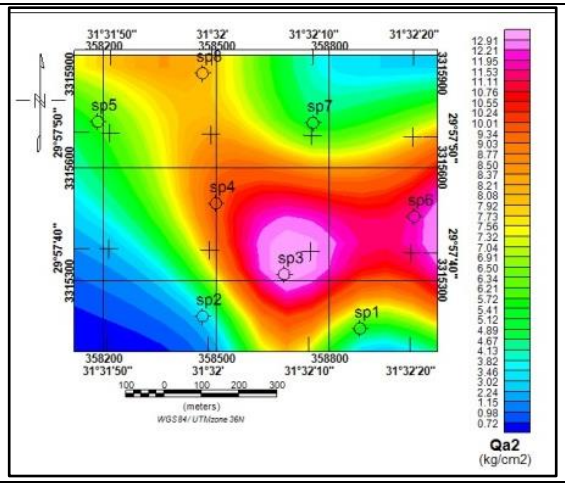

Fig.14b: Allowable Bearing Capacity colored image of the second layer in the spot area.

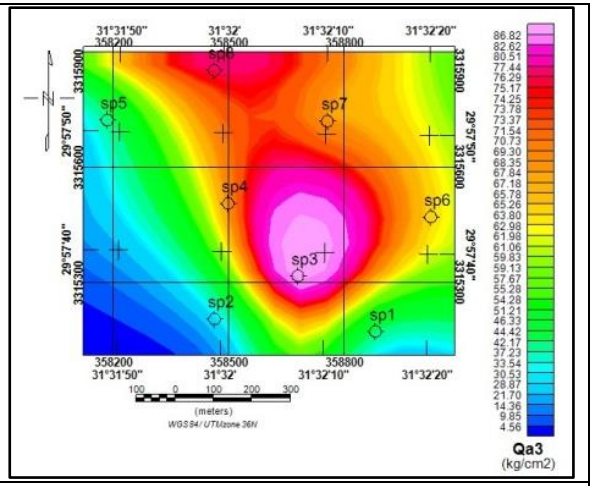

Fig.14c: Allowable Bearing Capacity colored image of the third layer in the spot area.

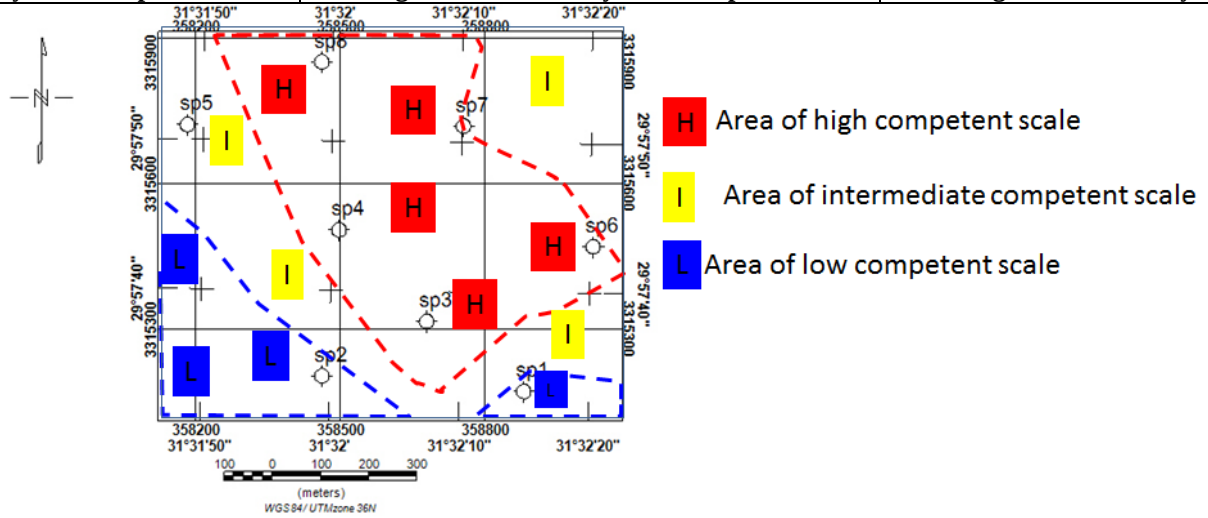

Fig. 15: distribution map of the Competence scale in the spot area.

6. References

Abd El-Rahman, M. M., 1989, Evaluation of the kinetic elastic moduli of the surface materials and applications to engineering geologic maps at Mabar- Risabah area , Dhamar Province, Northern Yemen: Egypt. J. Geol., Vol. 33, 1-2, pp. 229-250.

Abd El-Rahman, M. M., 1991, Rock material competence assessed by seismic measurements with emphasis on soil competence scale and application in some urban areas in Yeman. E.G.S. Proc. Of the 9th ann. Meet., pp. 206-228.

Abd Elrahman, M., Setto, I. And Elwerr (1992): Inferring mechanical properties of the foundation materials at the 2*P*nd. industrial zone, Sadat City, from Geophysical measurement, EGS. Proc. Of the 10*P*th. Ann.Meet. 10, PP.50-62.

Araffa, S.A.,2016 , Contribution of geophysical studies on detection of the Petrified Frost Qattamiya, Cairo, Egypt, Egyptian Journal of Petroleum

Bowles, J. E. 1984, Physical and geotechnical properties of soils. McGraw Hill Inter. Book Company, London, 2nd ed., 587 p.

Brace, W. F., 1965, Some new measurements of linear compressibility of rocks, J. Geophys. Res., vol. 70 (pp. 391-398)

CONCO, 1987, Geological map of Egypt 1:500 000. NH 36 NW. Cairo sheet.

Dutta, N. P. (1984): Seismic refraction method to study the foundation rock of a dam. J. Geophys. Prosp ., Vol. 32, pp. 1103-1110.

Grant, F, S. and West, G, F. 1965, Interpretation theory in applied geophysics. New York. McGraw-Hill Book Co., Inc.

Imai, T., Fumoto, H., and Yokota, K. 1976, P- and S- wave velocities in subsurface layers of ground in Japan. Urawa Research Inst., Tokyo.

Kaarsberg E A. 1966, Determination of elastic constants of an isotropic solid using a plate velocity measurement, Geophysics , vol. 31 (pg. 984-6).

Kelly, W. E. and Mares, S. 1993, Applied geophysics in hydrogeological and engineering practice. Elsevier sci. Publ. B. V., 289 p.

Koefoed, O. , 1955, On the effect of Poisson's ratio of rock strata on the reflection coefficients of plane waves, Geophys. Prospect. vol. 3 (pg. 381-7).

Nassif, M. S., 2018, Middle-Upper Eocene Benthic foraminiferal Biostratigraphy across Cairo-Sukhna district, North Eastern Desert, Egypt. IOSR Journal of Applied Geology and Geophysics (IOSR-JAGG) e-ISSN: 2321–0990, p-ISSN: 2321–0982.Volume 6, Issue 1 Ver. II (Jan. – Feb. 2018), PP 43-53

Othman A.A. 2005, Construed geotechnical characteristics of foundation beds by seismic measurements *Journal of Geophysics and Engineering*, Volume 2, Issue 2, 2005126–138,

Parry R. H. 1977, Estimating bearing capacity of sand from SPT values. JGED, ASCE., GT. 9, Vol. 103, pp. 1014-1043.

Shukri, M. M., 1954, The geology of the desert east Cairo. Bull.L, Institut Desert d, Egypt, Tome 3 (2): pp.89-105.

Shukri, N. M., Akmal, M. G. 1953, The geology of Gebel El Nasuri and Gebel El Anqabia area, Cairo–Suez distric. Bull Soc Geogr d'Egypte 26 (276):276–276

Sjoren B O, SangbergJ., 1979, Seismic classification of rock mass qualities, Geophys. Prospect., vol. 27 pp. 10-40

Telford, W.M., Geldast, L.P., Sheriff, R.E. and Keys, D.A. 1976, Applied geophysics, Cambridge, Cambridge Univ. Press, 860 p.

Thomson, L. 1986, Weak elastic anisotropy. Geophys. Prosp. Vol. 51, pp. 1954-1966.

Zittel, K.A., 1883, "Bitrage Zur Geology und Palontologie de libyschen wuste un angrenzenden Gebiete von Egypten". Paleontographica, 30: 147 pp., Kasse